FULL PAPER

From a Molecular Single-Source Precursor to a Selective High-Performance $RhMnO_x$ Catalyst for the Conversion of Syngas to Ethanol

Phil Preikschas,[a] Julia Bauer,[a] Xing Huang,[b] Shenglai Yao,[c] Raoul Naumann d'Alnoncourt,[a] Ralph Kraehnert,[a] Annette Trunschke,[b] Frank Rosowski,[a,d] and Matthias Driess*[a,c]

Abstract: The first molecular carbonyl RhMn cluster $Na_2[Rh_3Mn_3(CO)_{18}]$ **2** with highly labile CO ligands and predefined Rh-Mn bonds could be realized and successfully used for the preparation of the silica (davisil)-supported $RhMnO_x$ catalysts for the conversion of syngas (CO, H_2) to ethanol (StE); it has been synthesized through the salt metathesis reaction of $RhCl_3$ with $Na[Mn(CO)_5]$ **1** and isolated in 49 % yields. The dianionic Rh_3Mn_3 cluster core of **2** acts as a molecular single-source precursor (SSP) for the low-temperature preparation of selective high-performance $RhMnO_x$ catalysts. Impregnation of **2** on silica (davisil) led to three different silica-supported $RhMnO_x$ catalysts with dispersed Rh nanoparticles tightly surrounded by a MnO_x matrix. By using this molecular SSP approach, Rh and MnO_x are located in close proximity on the oxide support. Therefore, the number of tilted CO adsorption sites at the $RhMnO_x$ interface increased leading to a significant enhancement in selectivity and performance. Investigations on the spent catalysts after several hours time-on-stream revealed the influence of rhodium carbide RhC_x formation on the long-term stability.

Introduction

Depletion of fossil fuel resources and rising crude oil prices lead to one of the most important scientific challenges of the 21st century – finding a promising alternative to petroleum-derived fuels. In this manner, ethanol is being considered as a potential alternative fuel or as fuel additive in automobiles.[1,2] The use of bioethanol produced by fermentation of biomass-derived sugars could lead to rising food prices and ethical problems.[3]

A promising alternative would be a process to synthetic ethanol, which could also be used as a feedstock for synthesis of a wide range of industrial chemicals, polymers, or as fuel in direct alcohol fuel cells.[4,5] The direct conversion of syngas to ethanol (StE) is a promising process utilizing coal, natural gas, or preferably biomass as carbon source for syngas generation. To make this process technically and commercially feasible, a selective high-performance catalyst for StE is highly desired.

As supported rhodium is the only monometallic catalyst that has demonstrated selectivity toward ethanol,[6,7] a wide range of promoters were tested, e. g. containing Fe,[8,9] Mn,[10] Li,[11] and even rare earth oxides, such as CeO_2 or Pr_6O_{11}.[12] From these studies, it turned out that Mn-promoted Rh catalysts are among the best systems known as yet for the conversion of syngas to ethanol and other C_{2+} oxygenates (e. g., acetaldehyde, acetic acid).[10] By using Mn as a promoter, a higher selectivity toward ethanol as well as an increase of CO conversion can be achieved. According to a recent review by Luk *et al.*,[2] the most performant Mn-promoted Rh catalysts in the conversion of StE showed an ethanol selectivity of 17.7 % and an overall C_{2+} oxygenate selectivity of 42.0 % at a CO conversion of 17.0 %. These catalysts were prepared by incipient wetness impregnation of the respective metal nitrates and subsequent calcination.[13]

Despite these promising results, the production of undesirable methane is still present with selectivities up to 43.7 %.[13] A theoretical study has shown that methane formation is inevitable on supported RhMn catalysts due to a low activation barrier for methanation.[14] However, the number of active sites for the methane formation decreases, if Mn is in close proximity to Rh.[15,16] These close interactions not only decrease the selectivity toward methane but also promote the formation of ethanol by modifying the surface structure for the conversion of StE. One promising strategy to bring about Rh and Mn in close proximity could be achieved by the molecular single-source precursor (SSP) approach with a well-defined Rh:Mn ratio and Rh-Mn bonds. Encouraged by the recent progress in using molecular SSPs for solid catalyst design and preparation,[17] we synthesized the first molecular RhMn SSP and investigated its suitability to produce more selective RhMn-based StE catalysts. Here we present the synthesis and characterization of the carbonyl heterobimetallic $Na_2[Rh_3Mn_3(CO)_{18}]$ cluster **2** that acts as a suitable SSP for the low-temperature preparation of a silica-supported $RhMnO_x$

[a] P. Preikschas, J. Bauer, Dr. R. Naumann d'Alnoncourt, Dr. R. Kraehnert, Dr. F. Rosowski, Prof. Dr. M. Driess
BasCat – UniCat BASF JointLab
Technische Universität Berlin
Hardenbergstraße 36, Sekr. EW-K01, 10623 Berlin (Germany)
E-Mail: matthias.driess@tu-berlin.de
[b] Dr. X. Huang, Dr. Annette Trunscke
Department of Inorganic Chemistry
Fritz-Haber-Institut der Max-Planck-Gesellschaft
Faradayweg 4-6, 14195 Berlin (Germany)
[c] Dr. S. Yao, Prof. Dr. M. Driess
Metalorganic Chemistry and Inorganic Materials, Department of Chemistry
Technische Universität Berlin
Strasse des 17. Juni 135, Sekr. C2, 10623 Berlin (Germany)
[d] Dr. F. Rosowski
BASF SE, Process Research and Chemical Engineering
Heterogeneous Catalysis
Carl-Bosch-Strasse 38, 67056 Ludwigshafen (Germany)

Supporting information for this article is given via a link at the end of the document.

catalyst, which shows the highest selectivity for the conversion of syngas to ethanol reported to date.

Results and Discussion

Synthesis and Characterization of a Suitable Molecular Single-Source Precursor to Give $RhMnO_x$ Catalysts

The novel Rh_3Mn_3 cluster **2** was synthesized from the salt metathesis reaction of $RhCl_3$ with $Na[Mn(CO)_5]$ **1** in THF as a fine black powder in 49 % yields (Scheme 1). The composition of **2** was confirmed by elemental analysis; **2** is sensitive towards air and readily soluble in protic and nonprotic polar solvents (ethanol, acetonitrile, acetone, THF, and DMF).

$$\underset{\mathbf{1}}{7\ Na[Mn(CO)_5] + 3\ RhCl_3} \xrightarrow[-\ CO]{-\ 5\ NaCl} \underset{\mathbf{2}}{Na_2[Rh_3Mn_3(CO)_{18}]} + 2\ [Mn(CO)_4Cl]_2$$

Scheme 1. Synthesis of $Na_2[Rh_3Mn_3(CO)_{18}]$ **2**.

Single crystals suitable for an X-ray diffraction (XRD) analysis were obtained by diffusion of pentane vapors into a concentrated solution of **2** in THF at –37 °C. Compound **2** crystallized as a separate ion-pair; the dianionic Rh_3Mn_3 cluster core consists of an array of the six metal atoms, which are distributed as a central triangle of three rhodium atoms with a bridging manganese atom on each site (Fig. 1).

This hexanuclear metal core has a nearly planar geometry with three roughly straight angles of Mn-Rh-Mn (av. 174.0(9)°), leading to a mean deviation of 0.14 Å to the best plane. The latter cluster core is stabilized by 12 terminal and 6 bridging CO ligands that additionally link the Mn atoms with the Rh_3 subunit. These bridging CO ligands protrude out of the plane and are coordinated to a Na ion on each site resulting in a small bending to the middle of the hexanuclear Rh_3Mn_3 metal core (Fig. S1 in *Supporting Information*). The terminal CO ligands are distributed over the Mn as well as Rh atoms. Each Mn atom carries three terminal CO ligands, one of them within and the others out of the plane. The remaining three terminally bound COs are in-plane and each attached to a Rh atom. They are slightly bended with an av. Rh-C-O bond angle of 174.1°. The central Rh_3 triangle has an almost equilateral structure with an average bond angle of 60.00(7)°. The mean Rh–Rh distance of 2.870(3) Å is significantly longer than those observed in other rhodium species, such as $Rh_3(\mu\text{-}CO)_2(Cp)_3$ (av. 2.59 Å) or $Rh_3(\mu\text{-}CO)_3(Cp)_3$ (av. 2.65 Å).[18,19] The six Rh-Mn bonds have an average bond length of 2.638(4) Å and are slightly shorter than the other reported Rh-Mn bond (2.70 Å).[20] The dianionic Rh_3Mn_3 cluster core of **2** is highly symmetric with an overall C_3 symmetry, which is in accordance with a singlet resonance observed in the ^{55}Mn-NMR spectrum at δ = -2702.5 ppm.

The structural features of the Rh_3Mn_3 core of **2** are reminiscent of the reported hexanuclear $Na_3[Cu_3Fe_3(CO)_{12}]$ and $Os_6(CO)_{21}$ compounds.[21–25]

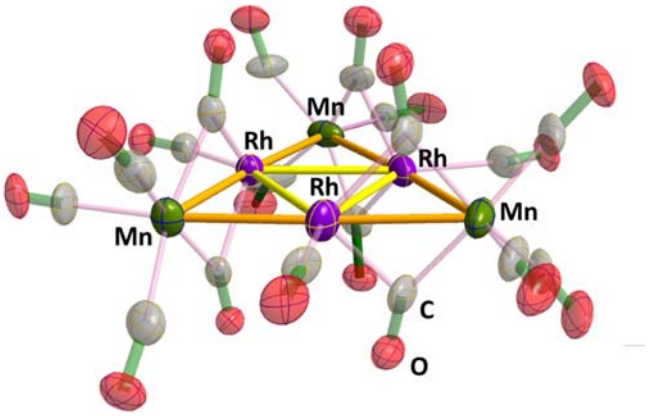

Figure 1. Molecular structure of the cluster dianion of **2**. Thermal ellipsoids are drawn at 50 % probability level. Sodium cations and stabilizing THF molecules are omitted for clarity. An overall image is provided as Figure S1 in the *Supporting Information*. Selected distances (Å) and angles (°): Rh1-Rh2 2.877(3), Rh1-Mn1 2.640(6), Rh1-Rh2-Rh3 60.26(7), Mn1-Rh1-Mn3 173.08(16).

Transformation of Supported Precursors into StE Catalysts

Compound **2** was used as a molecular SSP for three different silica-supported $RhMnO_x$ catalysts. In the first case, a solution of **2** in acetonitrile was impregnated *via* incipient wetness method on davisil, a commercially available silica with a BET surface area of 480 m^2/g.

FT-IR measurements confirmed the integrity of **2** on the silica-support (Fig. S2). The present Rh–Mn bonds in **2** could be advantageous for the preparation of a metallic Rh catalyst with a close proximity to MnO_x sites generated through low-temperature decomposition. To identify the proper conditions for such a mild transformation of supported **2**, a temperature-programmed decomposition (TPDe) investigation was performed after impregnation (Fig. S3). A two-step decarbonylation could be observed which begins at approx. 70 °C and reaches its maximum at 96.4 °C. This might be attributed to the weaker bonded bridging CO ligands, whereas the decarbonylation of the terminal CO ligands occurs at the second maximum at 113 °C. Based on these observations, silica-supported **2** has been transformed into the $NaRhMnO_x/SiO_2$ catalyst **3** with a nominal loading of 1.25 wt% Na, 1.50 wt% Mn, 2.80 wt% Rh by a low-temperature decomposition in 10 % dihydrogen with two heating steps at 75 and 115 °C, respectively. These temperatures are far below of a classical preparation route using single metal (Rh, Mn) nitrates (350 °C) which might avoid the sintering of Rh particles at temperatures above StE reaction conditions (260 °C).

To investigate the role of sodium on the RhMn system, two different routes to sodium-free $RhMnO_x/SiO_2$ catalysts were pursued: a) the Na ions were removed from as-synthesized **3** by a Soxhlet extraction with methanol leading to a sodium-free $RhMnO_x/SiO_2$ catalyst **4**, and b) the Na cations in **2** were replaced by the trimethylbenzylammonium cation to give another sample of sodium-free $RhMnO_x/SiO_2$ catalysts **5**. The absence of sodium in both catalysts was confirmed by elemental analysis *via* inductively coupled plasma optical emission spectrometry (ICP-OES).

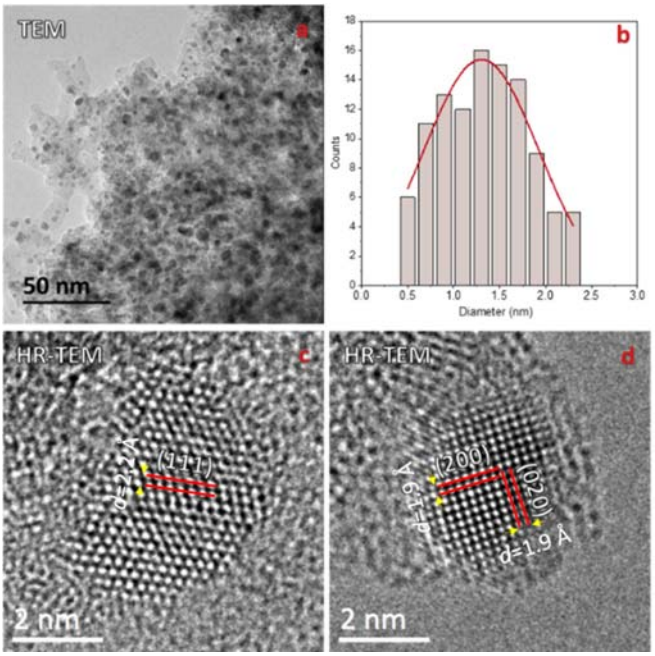

Figure 2. (HR-)TEM images of the as-prepared silica-supported $RhMnO_x/SiO_2$ catalyst **5** after reduction in H_2 at 260 °C: a,b) Rh nanoparticles are homogenously dispersed on silica and surrounded by a MnO_x matrix; c,d) the indicated lattice fringes of the crystalline particles correspond to the fcc{111}, fcc{200} planes of metallic Rh.

Powder XRD measurements were accomplished for phase identification of the as-synthesized materials **3**–**5** (Figs. S4 and S5). No specific reflections could be identified due to the limit of XRD for the detection of supported, crystalline nanoparticles (around 3.0 nm).[26] On this account, high-resolution transmission electron microscopy (HR-TEM) and annular dark-field scanning transmission microscopy (ADF-STEM) combined with energy-dispersive X-ray (EDX) mapping were conducted to determine the structure, morphology and atomic composition of **5**.

The overview TEM image showed relatively small nanoparticles with a mean particle size of 1.55 nm, which are homogeneously distributed on the silica-support (Fig. 2a). Lattice fringes analyses were then performed on the HR-TEM images to determine the atomic structure of the nanoparticles, which are size-representative according to the particles size distribution in Figure 2b. The crystalline particles show lattice fringes with *d*-spacings of 2.2 (Fig. 2c), 1.9 Å (Fig. 2d). They are consistent with fcc{111}, fcc{200} planes of metallic Rh in the space group Fm-3m (Fig. 2c,d). Metallic Mn or crystalline MnO_x particles could not be observed. This leads to the assumption that Mn is in an amorphous phase. In addition, it is not possible to distinguish between MnO_x and SiO_2 due to the low loading and the weak phase contrast compared to that of the silica-support.

The structural information based on lattice fringes are not sufficient to differentiate between metallic Rh and RhMn alloy particles. Therefore, ADF-STEM in combination with EDX was conducted to investigate the composition of catalytic particles. The ADF-STEM images recorded from three different domains

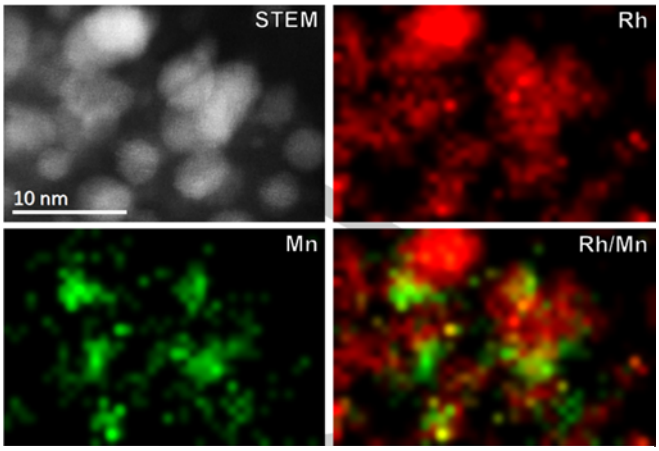

Figure 3. Composition analysis of the as-synthesized $RhMnO_x/SiO_2$ catalysts **5** after reduction in H_2 at 260°C. ADF-STEM with EDX mapping: Small particles of metallic rhodium (red) are closely contacted to a MnO_x species (green). No separated MnO_x or Rh nanoparticles could be observed.

show homogeneously dispersed nanoparticles with mean particles sizes of 1.30, 2.80 and 1.55 nm in the domains 1, 2 and 3 (Fig. S10), respectively. It also confirms a narrow size distribution of the synthesized nanoparticles (Fig. S10). The composition analyses were focused on domain 2, since particles smaller than 2 nm are difficult to study due to the insufficient EDX signal. The EDX mapping (Figure 3; for more EDX mappings (Fig. S11) and an EDX line-scan profile (Fig. S12) indicate homogeneously dispersed Rh nanoparticles, which are surrounded by a finely distributed manganese species. Thus, Rh is in close proximity to manganese and no separated Rh or MnO_x particles are found in all four domains (Figs. 3 and S10).

Since no crystalline Mn particles are observed in ADF-STEM images, it is assumed that Mn is in an oxidized state. This assumption was confirmed by XPS measurements without contact to an oxidative atmosphere (Fig. S8) and is also known for related $RhMnO_x$ catalysts.[16] However, the chemical state of Mn under reaction conditions is controversially discussed assuming that zero-valent Mn atoms might be alloyed with Rh.[14] Furthermore, a theoretical study described RhMn alloys as active species in the conversion of StE.[27] In this study, it can be shown that the formation of a supported RhMn nanoalloy is unfavourable on silica supports.

Not even the use of $Na_2[Rh_3Mn_3(CO)_{18}]$ **2** as molecular SSP with both metals in low oxidation states and predefined metal-metal bonds led to the formation of an alloy. The considerations that a reduction of Mn is induced by a close proximity to Rh might be attributed to classical preparation methods with precursors bearing Mn in high oxidation states. In this case, it cannot be distinguished whether the oxidation state of Mn in as-synthesized catalysts is caused by the used metal precursor or through the oxidation by an oxide support. On this account, the decomposition of silica-supported $Na[Mn(CO)_5]$ **1** metallate bearing Mn in the low oxidation state of -1 could not lead to the preparation of a zero-valent Mn species. The weakly Brønsted acidic silanol groups are likely to cause the immediate oxidation of the metallate **1** (Fig. S9).

It is therefore suggested that the oxidation of Mn to give MnO_x species is inevitable on silica, even under reaction conditions.

Catalytic Performance of the As-synthesized $RhMnO_x$ Catalysts

The as-prepared materials **3**–**5** were tested as catalysts for the direct conversion of StE in a fixed-bed parallel test setup at common reaction conditions for syngas chemistry (GHSV = 3500 h^{-1}, p = 54.0 bar, and T = 243–260 °C; see *Experimental Section*). The catalysts were directly compared with a Mn-promoted Rh catalysts **6** prepared by incipient wetness impregnation of the respective metal nitrates and subsequent calcination at 350 °C, and Rh/SiO_2 **8** prepared in a similar fashion (Tab. S2). For this comparison, different CO conversion levels were realized by variation of the reaction temperature from 243–260 °C.

Compared to the monometallic Rh/SiO_2 catalyst **8** (X_{CO} = 4.8 %, S_{EtOH} = 6.5 %; Tab. S2), all Mn-promoted catalysts show a substantially higher activity and ethanol selectivity. The enhancement of the catalytic performance due to the close proximity between Rh and MnO_x was also observed for other reported $RhMnO_x$ catalysts.[13,28] The catalytic results show a lower CO conversion of the SSP-originated catalysts **3**–**5** compared to the 'traditionally' prepared catalyst **6**. This finding might be attributed to a reduced metal loading of 0.6 wt% Rh which was confirmed by ICP-OES. However, the catalysts **3**–**5** show an increase in ethanol selectivity compared to the reference catalyst **6** as well as the mentioned literature-reported catalysts at iso-conversion denoted with hollow symbols in Figure 4a. In the case of **5**, the selectivity towards ethanol could be substantially enhanced by a factor of 1.54 and is – to our knowledge – the highest reported ethanol selectivity compared to literature examples (Fig. 4b).[2,13,29–31] We reason that the enhancement in selectivity is due to a higher dispersion of Rh nanoparticles in a tightly surrounded MnO_x matrix in the SSP-originated catalysts **3**–**5**, because this situation can increase the number of tilted CO adsorption sites which, in turn, facilitate the formation of ethanol (Scheme. S1). In fact, previous IR studies suggested that CO adsorbs in a tilted manner at Rh-MnO_x interfaces.[32,33] Moreover, results from diffuse reflectance infrared Fourier transform spectroscopy (DRIFTS) and kinetic investigations confirmed the enhancement of ethanol selectivity due to the tilted adsorption mode on $RhMnO_x$ which promotes CO dissociation on Rh^0 sites.[13,28] Furthermore, density functional theory (DFT) calculations proposed the lowering of the activation barrier for CO insertion into adsorbed CH_x fragments due to a tilted adsorption.[14] The Na content in RhMn SSP has an influence on activity and selectivity but only at very low conversions. At higher conversions both SSP-originated catalysts **3** and **4** exhibit similar ethanol selectivities.

Methane is the main product for all tested catalysts and its selectivity is reduced by factors of 0.83, 0.92, and 0.84 for catalysts **3**–**5**, respectively. The lower methanation might also be attributed to the close proximity of Rh and MnO_x. With a methane selectivity of 37.1 %, the Na containing catalyst **3** lowers the methane formation in a significant amount compared to the reference catalyst **6** with 44.8 %. Further products are other light hydrocarbons, methanol and oxygenates, mainly acetaldehyde and acetic acid.

Stability of the Synthesized $RhMnO_x$ Catalysts

After several hours time-on-stream (TOS), the catalysts **3** (105 h; Fig. S14) and **5** (220 h; Fig. S15) show a slight decrease in CO conversion due to deactivation. In the case of **5**, a notable deactivation in the first 20 h TOS can be observed (X_{CO} = 27.7 to 17.5 %). After this initial deactivation phase, the catalyst remains quite stable after additional 200 h TOS. However, the selectivity patterns remain similar and a difference in ethanol selectivity was not observed (Tab. S2, entry 3 and 7). The aforementioned deactivation might be induced by the formation of some larger particles due to sintering (Fig. 5a). For those larger particles a local enrichment of C was observed by ADF-STEM with EDX

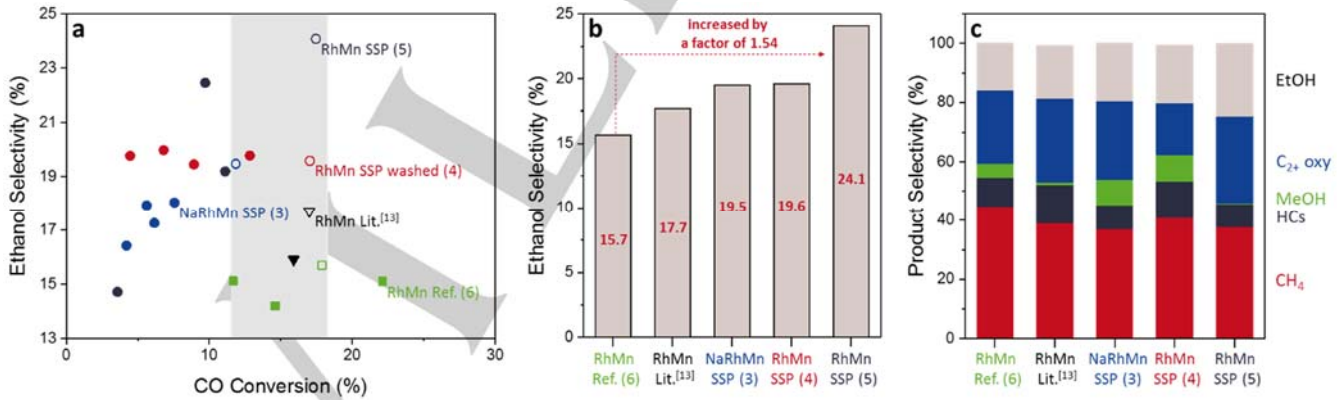

Figure 4. a) Ethanol selectivities (mol%) as function of CO conversions. Different CO conversion levels were realized by application of three different reaction temperatures. The range of iso-conversion which was chosen to compare the product selectivities are highlighted in grey b,c) Product selectivities (mol%) of measurements points marked with a hollow symbol at iso-conversion (11–16 %). The CO_2 selectivity is not shown here, as it is below 1 % for all tested catalysts. Measuring conditions: 243–260 °C, 54.0 bar, $p(H_2)$ = 32.4 bar, p(CO) = 10.8 bar, GHSV 3500 h^{-1}. CH_4, HCs, MeOH, C_{2+} oxy, and EtOH abbreviate methane, hydrocarbons, methanol, C_{2+} oxygenates, and ethanol, respectively. S(C_{2+} oxy) mainly includes acetaldehyde and acetic acid. For more details about the products, see Tab. S2 in *Supporting Information*.

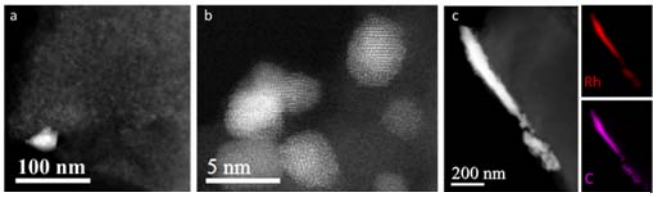

Figure 5. a,b) ADF-STEM images of the spent catalyst **5**: after 220 h TOS, some big particles are formed due to sintering but most of the particles remain relatively small. c) EDX mapping and EELS measurements (Figure S13) suggest the presence of a carbide phase in the bigger particles.

mapping (Fig. 5c), while respective EELS measurements suggest the presence of a rhodium carbide RhC_x phase (Fig. S13). However, most of the particles remain relatively small (Fig. 5b), which is the reason for the long-term stability of the system.

Conclusions

In summary, the first carbonyl RhMn cluster **2** with highly labile CO ligands and predefined Rh–Mn bonds could be realized and successfully used for the preparation of the silica (davisil)-supported $RhMnO_x$ catalysts **3**–**5**. The utilization of **2** as molecular SSP facilitates the formation of small Rh nanoparticles embedded in a finely distributed MnO_x matrix. This close proximity between Rh and MnO_x leads to a superior selectivity towards ethanol and also to a lower methane formation compared to reference as well as reported $RhMnO_x$ catalysts. The RhMn SSP catalysts **3**–**5** show the best performance of a Mn-promoted Rh catalyst in the conversion of StE reported as yet. In addition, the usage of the RhMn cluster **2** as molecular SSP shows that the formation of a RhMn alloy is unfavorable on silica supports due to the inevitable oxidation of Mn.

Long-term stability tests showed only a moderate deactivation after an initial phase and several hours TOS. Based on ADF-STEM images with EDX mapping and EELS measurements, the formation of a rhodium carbide RhC_x phase is suggested which might lead to the deactivation of $RhMnO_x$ catalysts besides sintering of Rh nanoparticles.

The molecular SSP approach is therefore a powerful tool for solid catalysts design resulting in highly dispersed metals embedded in oxide matrices and might lead to a better understanding of catalyst structure-function relationships. In this manner, it might be applicable to other catalysts systems, such as silica-supported $RhFeO_x$ and $Rh(Mn,Fe)O_x$ catalysts by choosing suitable molecular SSPs, e.g. $Na[RhFe_2(CO)_{11}]$ or a [RhMnFe] carbonyl cluster.[34]

Experimental Section

General Considerations. All manipulations involving air- and moisture sensitive organometallic compounds were carried out under an atmosphere of dry, oxygen-free argon by using standard Schlenk techniques or glove boxes (MBraun LABmaster Pro) under a purified nitrogen or argon atmosphere. There solvents were taken from a solvent purification system (MBraun SPS-800) or purified using conventional procedures, freshly distilled under argon atmosphere and degassed prior to use.

NMR spectroscopy. NMR samples of air- and moisture-sensitive compounds were prepared in a J. Young NMR tube (sealed with a polytetrafluoroethylene valve) under nitrogen atmosphere inside a glove box. The deuterated solvents were dried over a 4 Å molecular sieves and degassed prior to use. The ^{13}C- and ^{55}Mn-NMR spectra were recorded on a Bruker AvanceIII (^{13}C: 125 MHz, ^{55}Mn: 124 MHz) spectrometer. The $^{13}C\{^1H\}$-NMR spectra were referenced to residual solvent signal as internal standards (acetonitrile-d_3: δ_C = 1.32 ppm) and the ^{55}Mn-NMR spectra were referenced to a solution of $KMnO_4$ in D_2O. The abbreviations used to denote the multiplicity of the signals are singlet (s) and multiplet (m).

FT-IR spectroscopy. IR spectra (4000–400 cm^{-1}) of air- or moisture sensitive samples were recorded on a Nicolet iS5 spectrometer inside a glove box. Solid samples were measured with an attenuated total reflectance sampling technique and are directly placed on an ATR crystal (diamond). All other samples were placed as solid or as drop of a solution on an ATR crystal (diamond) of a Bruker ALPHA FT-IR spectrometer. The spectra were collected as data point tables by using OMNIC (Thermo Fisher Scientific Inc.) or OPUS (Bruker Corporation) software and were analyzed with Origin (OriginLab Corporation). Intensities of absorption bands were assigned on basis of visual inspection and were abbreviated as very strong (vs), strong (s), medium (m) and weak (w).

Mass spectroscopy. Mass spectra were recorded using HR-ESI-MS-method on an LTQ Orbitrap XL spectrometer.

Elemental analyses. The determination of the mass fractions of carbon, hydrogen, nitrogen and sulfur were carried out on a Thermo Finnigan FlashEA 1112 Organic Elemental Analyzer. Air- or moisture sensitive samples were prepared in silver capsules in a glove box. Mass fractions of transition or alkali metals were achieved by ICP-OES with a Varian 715 Emission Spectrometer.

Single crystal X-ray diffraction. An analytically pure crystal was directly placed on a glass capillary with perfuorinated oil and measured in a cold nitrogen steam. The data of all measurements were collected on an Agilent Technologies SuperNova diffractometer at 150 K (Cu-K_α-radiation, λ = 1.5418 Å). The structure was solved by direct methods using SHELXT,[35] space group determinations were performed with XPREP and crystal structure refinements with SHELXL.[36] All aforementioned programs were handled with Olex^2 Crystallography Software.[37] The CCDC number 1868848 (**2**) contain the supplementary crystallographic data for this paper. The data can be obtained free of charge by contacting The Cambridge Crystallographic Data Centre, 12, Union Road, Cambridge CB2 1EZ, UK; fax: +44 1223 336033.

Powder X-ray diffraction. Powder X-ray diffraction (XRD) measurements were performed in Bragg-Brentano geometry on a D8 Advance II theta/theta diffractometer (Bruker AXS), using Ni-filtered Cu $K\alpha_{1,2}$ radiation and a position sensitive energy dispersive LynxEye silicon strip detector. The sample powder was filled into the recess of a cup-shaped sample holder, the surface of the powder bed being flush with the sample holder edge (front loading).

Electron microscopy. The samples were investigated by an aberration-corrected JEOL JEM-ARM200CF transmission electron microscope. The microscope is equipped with a high angle silicon drift EDX detector with the solid angle of up to 0.98 steradians from a detection area of 100 mm^2 that allows for EDX measurement.

Temperature-programmed decomposition (TPDe). TPDe-MS experiments were performed with a MicrotracBEL BelCat II setup, which was coupled to a mobile Pfeifer Vacuum QMG 220 mass spectrometer. In a typical experiment, a certain amount of the sample (around 50 mg) was placed in the sample cell inside a glove box and placed in the BelCat II setup. Helium was used as carrier gas with a flow rate of 54 mL/min and hydrogen was used for the decomposition with a flow rate of 6 mL/min. The temperature was linearly and continuously increased from RT to 873 K with a temperature ramp of 5 K/min. The reaction products were analyzed by the computer controlled quadrupole mass spectrometer.

X-ray photoelectron spectroscopy. XPS was measured on K-Alpha™ + X-ray Photoelectron Spectrometer (XPS) System (Thermo Scientific), with Hemispheric 180° dual-focus analyzer with 128-channel detector. X-ray monochromator is Micro focused Al-Kα radiation. For the measurement, the as-prepared samples were directly loaded on the sample holder for measurement. The data was collected with X-ray spot size of 200 µm, 20 scans for survey, and 50 scans for regions.

Catalytic Testing for Synthesis Gas Conversion. The catalytic testing of the syngas to ethanol reaction was performed in a 4-fold parallel testing unit. 0.5 g (~1 mL) catalyst with a particle size of 100-200 µm were loaded into each stainless steel reactor with an effective inner diameter of 6.25 mm. The reaction temperature was monitored by temperature sensors with three thermocouples along the catalyst bed.

Four mass flow controllers were used to adjust the flow rates of the inlet gases N_2 (99.999 %), CO (99.997 %), H_2 (99.999 %) and Ar (99.999 %, all Air Liquide). The CO feed line was equipped with a carbonyl trap in order to remove all metal carbonyls that might be formed by high pressure of CO in contact with stainless steel. The carbonyl trap consisted of a U-shaped ½" stainless steel tube filled with Al_2O_3 and heated to 170 °C by a heating sleeve.

Compounds in the effluent gas that condense below 180 °C were removed by a coalescence filter in the downstream oven. All remaining compounds in the effluent gas were analyzed with an online gas chromatograph (Agilent 7890B) equipped with two thermal conductivity detectors (TCD) and one flame ionization detector (FID) using He as the carrier gas. TCDs detect the inlet gases H_2, Ar, N_2, CO and in addition methane, CO_2 and H_2O. The FID is used to detect a large variety of paraffins, olefins and oxygenates (alcohols, acetaldehyde, acetic acid) with a combination of a Porabond Q and an RTX-Wax column. The carbon balance was between 96–102% for all measurements.

The catalysts are reduced *in-situ* at 54 bar, 265 °C with 5 % H_2 in N_2 for 1 h with a volume flow of 58.3 mL min^{-1}. Subsequently, the temperature was decreased to 243 °C and synthesis gas feedstock mixture containing $CO:H_2:N_2$:Ar (20:60:10:10%, v:v) was admitted. The volume flow was kept constant to achieve a GHSV of 3500 h^{-1}. The temperature was increased to 260 °C in three steps and subsequently decreased in the same manner. Each step was held constant for at least 15 h to allow the catalysts to equilibrate.

The obtained concentrations of all compounds were corrected for volume changes due to the reaction and the following N_2 dilution. Therefore, the mole fraction of Ar was used as inert internal standard according to equation 1.

$$n_{i,corrected} = n_{i,GC} \cdot \frac{n_{Ar,bypass}}{n_{Ar,reactor}} \quad (1)$$

$n_{i,corrected}$ is the corrected mole fraction of compound i. $n_{i,reactor}$ and $n_{i,bypass}$ are the mole fractions of compound i originally obtained by the gas chromatograph sampling the respective reactor or the bypass line.

Additionally, the results for all compounds detected by the FID were corrected using the mole fraction of methane obtained by FID and TCD according to equation 2.

$$n_i = n_{i,corrected} \cdot \frac{n_{methane,TCD}}{n_{methane,FID}} \quad (2)$$

n_i is the mole fraction of compound i that is finally used for further calculations. $n_{methane,TCD}$ and $n_{methane,FID}$ are the methane concentrations detected by TCD and FID after correction with the Ar standard (equation 1).

Carbon monoxide conversion X_{CO} was calculated indirectly from the summation of carbon numbers in all products rather than directly from the CO concentration as at small conversions the quantification of CO *via* TCD was not precise enough (equation 3).

$$X_{CO} = \frac{\sum n_j C_j}{n_{CO,0}} \quad (3)$$

$n_{CO,0}$ is the mole fraction of CO in the inlet gas and C_i is the carbon number of the product *i*. The selectivity *S* for each product *i* was determined based on the number of C atoms by equation 4.

$$S_i = \frac{n_i C_i}{\sum n_{i,j} C_{i,j}} \quad (4)$$

Synthesis of $Na[Mn(CO)_5]\cdot 0.5THF$ (1). Metallate **1** was synthesized by a modified literature-known preparation.[38] Metallic sodium (3.04 g, 0.133 mol) was cut in small pieces and suspended in 50 mL THF. This suspension was stirred at r.t. overnight. A yellow solution of manganese carbonyl $Mn_2(CO)_{10}$ (5.18 g, 13.3 mmol) in dry THF (45 mL) was added to the suspension. The mixture was stirred at r.t. for 72 h, during which time a color change from yellow over red to brown was observed. The suspension was then filtered and washed with additional 25 mL THF. The combined filtrates were evaporated to dryness in vacuum for 12 h, providing a light green solid. Yield: 4.60 g, 21.1 mmol, 81.2 % (Based on $Mn_2(CO)_{10}$). Note: THF molecules are still coordinated to Na, which was quantified by dynamic flash combustion analysis. This material was used for subsequent procedures without further purification. Elemental analysis (%): calcd for $C_7H_4O_{5.5}NaMn$: C, 33.10; H, 1.59 Found: C, 32.36; H, 1.86. $^{13}C\{1H\}$ NMR (125 MHz, CD_3CN, 298 K, ppm): δ = 238.68 (s, Mn-CO). ^{55}Mn NMR (124 MHz, CD_3CN, 298 K, ppm): δ = -2702.57. ESI-MS: m/z: calcd for $[M–Na]^-$: 194.9, found: 194.9. IR (ATR, cm^{-1}): ν = 1936 (w), 1884 (m), 1826 (s).

Synthesis of $Na_2[Rh_3Mn_3(CO)_{18}]\cdot 2THF$ (2). Rhodium(III) chloride $RhCl_3$ (602.4 mg, 2.88 mmol) was suspended in 100 mL ethanol (EtOH) and cooled down to -78 °C in an acetone/dry ice bath. A solution of $Na[Mn(CO)_5]$ (**1**, 1.79 g, 4.12 mmol) in 25 mL EtOH was added dropwise. The suspension was warmed up slowly to r.t. within 6 h, during which time a color change from green to dark brown and precipitation of a crystalline solid was observed. After stirring for 24 h, the mixture was filtered through a glass frit and the residue was washed two times with additional 10 mL of EtOH. The combined filtrates were evaporated under vacuum at 38 °C and dried in vacuum. This crude product was washed four times with 25 mL *n*-hexane and dried under vacuum overnight. The title compound was obtained as dark brown solid. Analytically pure black block-shaped crystals

were obtained by diffusion of pentane vapors into a concentrated and filtered solution in THF at -37 °C. Yield: 520.3 mg, 4.66 mmol, 48.6 % (based on $RhCl_3$). Elemental analysis (%): calcd for $C_{26}H_{16}O_{20}Na_2Mn_3Rh_3$: C, 26.70; H, 1.38 Found: C, 26.70; H, 1.37. $^{13}C\{1H\}$ NMR (125 MHz, CD_3CN, 298 K, ppm): δ = 210.69 (s, Mn-*C*O), 214.50 (s, Mn-*C*O), 216.67 (m, μ-*C*O). ^{55}Mn NMR (124 MHz, CD_3CN, 298 K, ppm): δ = -2606.78. ESI-MS: m/z: calcd for $[M\text{-}Na]^-$: 1000.3, found: 1000.4. IR (ATR, cm^{-1}): ν = 2077 (w), 2025 (m), 2001 (m), 1917 (m), 1798 (br, m). ATR-FTIR of a drop the *n*-hexane washing solution confirmed $[Mn(CO)_4Cl]_2$ as by-product. IR of $[Mn(CO)_4Cl]_2$ (ATR, cm^{-1}): 2115 (w), 2045 (m), 2006 (vs), 1934 (vs). Bands are in accordance to literature, IR (chloroform solution, cm^{-1}): 2104, 2047, 2006, 1977.[39] After serval days, $Mn_2(CO)_{10}$ crystallized from the solution in form of yellow needles due to the disproportion of $[Mn(CO)_4Cl]_2$ to $Mn_2(CO)_{10}$ and $MnCl_2$. The formation of $Mn_2(CO)_{10}$ was confirmed by single-crystal XRD. The lability of $[Mn(CO)_4Cl]_2$ in *n*-hexane solution and the subsequent disproportion was also observed elsewhere.[40]

Synthesis of $NaRhMnO_x/SiO_2$ SSP (3). A solution of **2** (141.1 mg, 0.12 mmol) in acetonitrile (3.70 mL) was added to 3.26 g SiO_2 (sieve fraction 100–200 µm) under mixing with a spatula. The addition of the solution was conducted in three steps á 1.23 mL which corresponded to the specific pore volume of the support (0.90 mL/g) according to the incipient wetness impregnation method. After impregnation, the silica-supported precursor was dried under high vacuum for 12 h at room temperature. The pre-catalyst was activated by thermal treatment in flowing 10 % H_2/Ar (total flow 500 mL/min). A temperature program in accordance to the TPDe studies (Fig. S2) was chosen (Tab. 1). The final $NaRhMnO_x/SiO_2$ catalyst (3) was kept under inert gas atmosphere prior use. Metal loadings by ICP-OES (wt%): 2.21 Rh, 1.34 Mn.

Table 1. Temperature Program of Catalyst Activation.

Step	Temperature (°C)	Holding Time (h)
1	75	4
2	115	4
3	260	1

Synthesis of $RhMnO_x/SiO_2$ SSP washed (4). The $NaRhMnO_x/SiO_2$ SSP catalyst (3) was washed with methanol by a soxhlet extraction. The washed pre-catalyst was dried in high vacuum yielding the final $RhMnO_x/SiO_2$ SSP (4). Metal loadings by ICP-OES (wt%): 1.82 Rh, 0.87 Mn.

Synthesis of $RhMnO_x/SiO_2$ SSP (5). The final $RhMnO_x/SiO_2$ SSP catalyst (5) was synthesized in a similar manner as catalyst **3**. Incipient wetness impregnation of a solution of **7** (252.2 mg, 0.197 mmol) in 3.6 mL THF on silica (1.362 g) in 3 steps, drying in high vacuum for 12 h at r.t. and activation in flowing 10 % H_2/Ar (total flow 500 mL/min) at 260 °C (ramp 5 K/min, holding time 2 h). Metal loadings by ICP-OES (wt%): 2.2 Rh, 0.70 Mn.

Synthesis of $RhMnO_x/SiO_2$ Reference Catalyst (6). The $RhMnO_2/SiO_2$ reference catalyst (6) was prepared according a previously reported procedure.[16] A aqueous solution of rhodium(III) nitrate $Rh(NO_3)_3 \bullet xH_2O$ and Manganese(II) nitrate $Mn(NO_3)_2 \bullet xH_2O$ in water (HPLC grade) was impregnated on silica (pre-treated at 550 °C in air for 6 h). A subsequent calcination in synthetic air at 350 °C was conducted providing the $Rh_2O_3MnO_x/SiO_2$ pre-catalyst. The precatalyst was reduced by H_2 at 265 °C *in-situ* prior the catalyst testing. Metal loadings by ICP-OES (wt%): 2.6 Rh, 1.3 Mn.

Synthesis of $[NBnzMe_3]_2[Rh_3Mn_3(CO)_{18}]$ (7). Benzyltrimethylammonium chloride $[NBnzMe_3]Cl$ (155.0 mg, 0.835 mmol) was suspended in 15 mL acetone and a solution of $Na_2[Rh_3Mn_3(CO)_{18}]$ (2, 133.5 mg, 0.120 mmol) in 10 mL acetone was added dropwise to the suspension. The suspension was stirred at room temperature for 24 h and filtered through a glass frit. The residue was washed with additional 10 mL of acetone. The combined filtrates were evaporated under vacuum at 45 °C and then dried in vacuum for 12 h. The crude product was washed three times with 5 mL toluene and dissolved in 10 mL THF. Evaporation of the solvent and drying in vacuum overnight led to a tacky compound which was not isolatable. Yield: 71.4 mg, 0.04 mmol, 31.8 % (Based on cluster **2**). This material was used for subsequent procedures without further purification. IR (ATR, cm^{-1}): ν = 2068 (w), 2020 (w), 1992 (m), 1958 (m), 1917 (m), 1793 (m). ESI-MS: m/z: calcd for $[M\text{-}NBnzMe_3]^-$: 1071.6, found: 1070.8.

Synthesis of Rh/SiO_2 Reference Catalyst (8). The Rh/SiO_2 reference catalyst (8) was prepared in a similar manner as reference catalyst **6**.[16] A aqueous solution of rhodium(III) nitrate $Rh(NO_3)_3 \bullet xH_2O$ in water (HPLC grade) was impregnated on silica (pre-treated at 550 °C in air for 6 h). A subsequent calcination in synthetic air was conducted providing the Rh_2O_3/SiO_2 pre-catalyst. The precatalyst was activated *in-situ* prior the catalyst testing. Metal loading by ICP-OES (wt%): 2.8 Rh.

Acknowledgements

This work was conducted in the framework of the BasCat collaboration between BASF SE, TU Berlin, Fritz Haber Institute of the Max Planck Society, and the Cluster of Excellence UniCat (EXC 314-2; financed by the Deutsche Forschungsgemeinschaft). We thank Dr. Somenath Garai for crystal structure refinement, Dr. Frank Girgsdies for XRD, Shuang Li for XPS measurements, and Stephen Lohr for technical assistance.

Keywords: Heterobimetallic Catalysis • Hydrogenation • Rhodium • Manganese • Oxygenates

[1] A. K. Agarwal, *Prog. Energy Combust. Sci.* **2007**, *33*, 233–271.
[2] H. T. Luk, C. Mondelli, D. C. Ferré, J. A. Stewart, J. Pérez-Ramírez, *Chem. Soc. Rev.* **2017**, *46*, 1358–1426.
[3] J. Hill, E. Nelson, D. Tilman, S. Polasky, D. Tiffany, *Proc. Natl. Acad. Sci. U. S. A.* **2006**, *103*, 11206–10.
[4] V. Subramani, S. K. Gangwal, *Energy & Fuels* **2008**, *22*, 814–839.
[5] M. Z. F. Kamarudin, S. K. Kamarudin, M. S. Masdar, W. R. W. Daud, *Int. J. Hydrogen Energy* **2013**, *38*, 9438–9453.
[6] P. C. Ellgen, M. Bhasin (Union Carbide Corp.), U.S. Patent 4096164A. **1976**.
[7] W. J. Bartley, T. P. Wilson (Union Carbide Corp.), U.S. Patent 4446251A, **1982**.
[8] F. Xue, W. Chen, X. Song, X. Cheng, Y. Ding, *RSC Adv.* **2016**, *6*, 35348–35353.
[9] M. Haider, M. Gogate, R. Davis, *J. Catal.* **2009**, *261*, 9–16.
[10] M. Ojeda, M. L. Granados, S. Rojas, P. Terreros, F. J. Garcia-Garcia, J. L. G. Fierro, *Appl. Catal. A Gen.* **2004**, *261*, 47–55.
[11] X. Mo, J. Gao, J. G. Goodwin, *Catal. Today* **2009**, *147*, 139–149.
[12] D. Yu-hua, C. De-An, T. Khi-Rui, *Appl. Catal.* **1987**, *35*, 77–92.
[13] W. Mao, J. Su, Z. Zhang, X.-C. Xu, W. Dai, D. Fu, J. Xu, X. Zhou, Y.-F. Han, *Chem. Eng. Sci.* **2015**, *135*, 312–322.

[14] D. Mei, R. Rousseau, S. M. Kathmann, V.-A. Glezakou, M. H. Engelhard, W. Jiang, C. Wang, M. A. Gerber, J. F. White, D. J. Stevens, *J. Catal.* **2010**, *271*, 325–342.
[15] Y. Choi, P. Liu, *J. Am. Chem. Soc.* **2009**, *131*, 13054–13061.
[16] M. Dimitrakopoulou, X. Huang, J. Kröhnert, D. Teschner, S. Praetz, C. Schlesiger, W. Malzer, C. Janke, E. Schwab, F. Rosowski, H. Kaiser, S. Schunk, R. Schlogl, A. Trunschke, *Faraday Discuss.* **2018**, *208*, 207–225.
[17] C. Panda, P. W. Menezes, M. Driess, *Angew. Chem. Int. Ed.* **2018**, *57*, 11130–11139.
[18] A. C. Bray, M. Green, D. R. Hankey, J. A. K. Howard, O. Johnson, F. Gordon, A. Stone, *J. Organomet. Chem.* **1985**, *281*, c12–c16.
[19] D. Braga, F. Grepioni, H. Wadepohl, S. Gebert, M. J. Calhorda, L. F. Veiros, *Organometallics* **1995**, *14*, 5350–5361.
[20] M. L. Aldridge, M. Green, J. A. K. Howard, G. N. Pain, S. J. Porter, F. G. A. Stone, P. Woodward, *J. Chem. Soc. Dalt. Trans.* **1982**, 1333.
[21] G. Longoni, M. Manassero, M. Sansoni, *J. Am. Chem. Soc.* **1980**, *102*, 7973–7974.
[22] M. J. Freeman, A. D. Miles, M. Murray, A. Guy Orpen, F. G. a. Stone, *Polyhedron* **1984**, *3*, 1093–1097.
[23] G. Doyle, K. A. Eriksen, D. Van Engen, *J. Am. Chem. Soc.* **1986**, *108*, 445–451.
[24] A. Bott, J. G. Jeffrey, B. F. G. Johnson, J. Lewis, *J. Organomet. Chem.* **1990**, *394*, 533–554.
[25] A. Antiaolo, F. A. Jalon, A. Otero, M. Fajardo, B. Chaudret, F. Lahozd, J. A. Lopezd, **1991**, 1861–1866.
[26] K. O'Connell, J. R. Regalbuto, *Catal. Letters* **2015**, *145*, 777–783.
[27] X. Ma, H. Deng, M.-M. Yang, W.-X. Li, *J. Chem. Phys.* **2008**, *129*, 244711.
[28] W. Mao, J. Su, Z. Zhang, X. C. Xu, D. Fu, W. Dai, J. Xu, X. Zhou, Y. F. Han, *Chem. Eng. Sci.* **2015**, *135*, 301–311.
[29] J. Liu, R. Tao, Z. Guo, J. R. Regalbuto, C. L. Marshall, R. F. Klie, J. T. Miller, R. J. Meyer, *ChemCatChem* **2013**, *5*, 3665–3672.
[30] G. Chen, C.-Y. Guo, X. Zhang, Z. Huang, G. Yuan, *Fuel Process. Technol.* **2011**, *92*, 456–461.
[31] D. Mei, R. Rousseau, S. M. Kathmann, V.-A. Glezakou, M. H. Engelhard, W. Jiang, C. Wang, M. A. Gerber, J. F. White, D. J. Stevens, *J. Catal.* **2010**, *271*, 325–342.
[32] X. Pan, Z. Fan, W. Chen, Y. Ding, H. Luo, X. Bao, *Nat. Mater.* **2007**, *6*, 507–511.
[33] W. M. H. Sachtler, M. Ichikawa, *J. Phys. Chem.* **1986**, *90*, 4752–4758.
[34] A. Ceriotti, G. Longoni, M. Manassero, M. Sansoni, R. Della Pergola, B. T. Heaton, D. O. Smith, *J. Chem. Soc., Chem. Commun.* **1982**, *3*, 886–887.
[35] G. M. Sheldrick, *Acta Crystallogr. Sect. A Found. Crystallogr.* **2015**, *71*, 3–8.
[36] G. M. Sheldrick, *Acta Crystallogr. Sect. C Struct. Chem.* **2015**, *71*, 3–8.
[37] O. V. Dolomanov, L. J. Bourhis, R. J. Gildea, J. A. K. Howard, H. Puschmann, *J. Appl. Crystallogr.* **2009**, *42*, 339–341.
[38] S. Banerjee, M. K. Karunananda, S. Bagherzadeh, U. Jayarathne, S. R. Parmelee, G. W. Waldhart, N. P. Mankad, *Inorg. Chem.* **2014**, *53*, 11307–15.
[39] E. W. Abel, I. S. Butler, *Trans. Faraday Soc.* **1967**, *63*, 45.
[40] C. H. Bamford, J. W. Burley, M. Coldbeck, *J. Chem. Soc. Dalt. Trans.* **1972**, 1846.

Entry for the Table of Contents

FULL PAPER

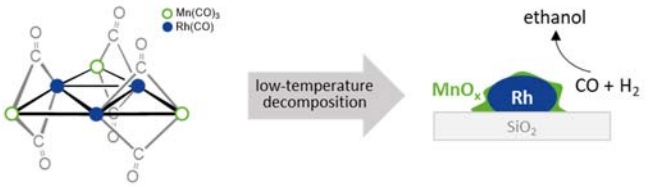

Catalysts Birth. The first carbonyl RhMn cluster $Na_2[Rh_3Mn_3(CO)_{18}]$ has been synthesized, structurally characterized and utilized as well-defined molecular single-source precursor (SSP) for the low-temperature preparation of selective high-performance RhMn catalysts for the conversion of syngas to ethanol (StE). Highly dispersed Rh nanoparticles in a tightly surrounded MnO_x matrix lead to a superior selectivity towards ethanol.

*Phil Preikschas, Julia Bauer, Xing Huang, Shenglai Yao, Raoul Naumann d'Alnoncourt, Ralph Kraehnert, Annette Trunschke, Frank Rosowski, and Matthias Driess**

Page No. – Page No.

From a Molecular Single-Source Precursor to a Selective $RhMnO_x$ High-Performance Catalyst for the Conversion of Syngas to Ethanol